

## Effect of polyelectrolyte spacer thickness on fluorescence decay kinetics of IgG-FITC conjugates near plasmonic silver film

© V.I. Stsiapura<sup>1</sup>, O.S. Kulakovich<sup>2</sup>, A.A. Maskevich<sup>3</sup>, D.V. Guzatov<sup>3</sup>, H.V. Demir<sup>4</sup>, S.V. Gaponenko<sup>2</sup>, S.A. Maskevich<sup>1</sup>

<sup>1</sup> International Sakharov Environmental Institute of Belarusian State University, 220070 Minsk, Republic of Belarus

<sup>2</sup> Stepanov Institute of Physics, Belarusian Academy of Sciences, Minsk, Belarus

<sup>3</sup> Yanka Kupala State University of Grodno, 230023 Grodno, Republic of Belarus

<sup>4</sup> Bilkent University, Bilkent, TR-06800 Ankara, Turkey

e-mail: stsiapura@gmail.com

Received September 07, 2023

Revised September 07, 2023

Accepted October 13, 2023

Enhancement of fluorescence near metallic nanostructures can significantly improve sensitivity of fluorescence-based detection methods and this effect has found wide applications in diagnostics and biosensors development. In the current paper we studied fluorescence decay kinetics of immunoglobulin G conjugates with fluorescein isothiocyanate near plasmonic silver film formed by colloidal nanoparticles having size of  $\sim 40$  nm. The emission kinetics was found to depend on thickness of a spacer composed from cationic/anionic polyelectrolytes (number of layers changed from 1 to 7), that separated fluorescent conjugate from the plasmonic film. Multiexponential fluorescence decay kinetics was modeled by continuous lifetime distribution of emitting centers using maximum entropy method. Based on theoretical calculations of radiative transition rate of fluorescent molecules near metal colloids we estimated ensemble-averaged fluorescence quantum yields of conjugates, located at different distances to plasmonic film, and found that the fluorescence enhancement for the conjugates near colloid nanoparticles was determined by changes in excitation efficiency but not due to growth of the emission quantum yield.

**Keywords:** nanoplasmonics, fluorescence decay, maximum entropy method, colloid nanoparticle, fluorescein isothiocyanate, immunodiagnosics.

DOI: 10.61011/EOS.2023.10.57765.5544-23

### Introduction

In order to achieve high sensitivity in immunodiagnosics, fluorescence-based methods are widely used, whereas substrates tested are various solid-phase systems containing plasmonic particles of silver and gold [1–11]. Such systems exhibit localization of electromagnetic radiation of an incident light wave near the surface of metallic nanoparticles (NP), thereby finally allowing increasing the intensity of a recorded signal of the fluorescent labels such as fluorescein isothiocyanate (FITC). The nanostructured plasmonic films are created on the surface of various dielectric materials as per universal technologies of electrostatic deposition of silver nanoparticles (Ag NP), as developed in [7,12–15]. This method is used in the paper [15] for creating metalized plasmonic coating in standard 96-well ELISA plates, thereby noticeably increasing sensitivity of the Immunofluorescence method for determination of the prostate-specific antigen. The intensity of the recorded fluorescence signal in the Ag NP presence was increased in 2–3 times in comparison with a signal obtained during immobilization of the test system on an intact surface of the polystyrene ELISA plate; whereas the signal-to-noise ratio was increased by

up to two times. Then, in the papers [16,17] the authors studied spectral and kinetical characteristics of fluorescence of immobilized immunoglobulin G conjugate with FITC (IgG-FITC) depending on the surface density of Ag NPs deposited on a bottom of the plate wells. The surface density of Ag NPs and their production technology were optimized.

It is shown that increase in the fluorescence intensity of the label on the metalized ELISA plate in 3–10 times depending on optical density of the silver film is predominantly related to the plasmonic effect. Seven times decrease of IgG-FITC fluorescence decay lifetime in the presence of plasmonic nanoparticles, increase in IgG-FITC fluorescence excitation efficiency within the plasmonic band located at 420–430 nm and significant decrease in the half-width of the fluorescence spectra have been recorded.

Metal-dielectric structures always lead to reduction of the excited state decay lifetime of nearby quantum systems (fluorophores). It is noteworthy that decrease in the excited state lifetime can be accompanied both by decrease or increase in the fluorescence intensity [18]. If an initial value of the fluorescence quantum yield for fluorophore is low ( $\Phi_0 \ll 1$ ), then changed probability of the radiative

and nonradiative decay processes in the excited state due to interaction with plasmons can result in increase in the emission quantum yield ( $\Phi > \Phi_0$ ). It is the most obvious in electroluminescence of plasmonic structures, wherein increase in a luminescent signal is fully determined by increase in the quantum yield [19,20]. In case of emitters with an intrinsically high fluorescence quantum yield  $\Phi_0 \sim 1$ , the presence of metal results in reduction of the value of the quantum yield  $\Phi < \Phi_0$ . However, there is a quite wide set of experimental conditions, when the fluorescence intensity of such emitters does not decrease, while the lifetime of the excited state is significantly shortened.

If the reduction of the lifetime of a fluorophore near the metal-dielectric nanostructures is caused by the growth of rate constant of the radiative transition, then one can expect reduction in probability of side photo-stimulated processes resulting in luminophore degradation while the fluorescence signal level will be unchanged. The reduction of the lifetime of the excited state of fluorophore by means of the metal-dielectric nanostructures can decrease the influence of the concentration effects on fluorescence quenching, which has been noted for FITC-labelled biomolecules [1,15] and rare-earth ions [21]. An important role of effects related to concentration quenching and their influence on the fluorescence intensity can be for IgG-FITC conjugates, when there are several fluorophore molecules per one protein molecule.

Traditionally, in the immunodiagnostics using the spectral luminescent methods, intensity is the main measured characteristic of fluorescence, which is considered to be linearly dependent on the concentration of a substance analyzed, for example, IgG-FITC [22]. However, the effects related to inhomogeneity of fluorophores microenvironment, their low photo-stability and concentration quenching result in a complicated dependency between the analyte concentration and luminescence intensity. Using the metal nanoparticles for fluorescence enhancement [23], wherein the enhancement effect substantially depends on the fluorophore-metal distance, results in even larger heterogeneity of the studied system, and characterization of the system using only one parameter — the intensity averaged over the fluorophores ensemble — can be insufficient.

The fluorescence decay kinetics data can be used to increase sensitivity and provide additional information about the properties and behavior of the system characterized by the structural and dynamic heterogeneity of emitting centers [24,25]. This approach is widely used in developing test systems for immunology analysis based on lanthanoids [26,27], as well as for investigating the mechanism of plasmon-enhanced fluorescence [23,28,29]. However, despite significant development of the mathematical methods of analysis of the fluorescence decay data [30,31], complexity of its interpretation is still a limiting factor preventing wider use of time-resolved fluorescence spectroscopy methods in practical applications of immunodiagnostics (except for the case of lanthanides ions characterized by emission kinetics in microsecond range).

In the present paper, we have experimentally investigated the fluorescence decay kinetics of the IgG-FITC conjugates immobilized on the surface of the metal-dielectric film, wherein the protein layer and the layer of colloidal Ag NPs of the size of 40 nm were spaced apart by alternating polyelectrolyte (PE) layers with a number of the layers from 1 to 7. In order to interpret the obtained results, the FITC luminescence decay curves were analyzed by multiexponential model and lifetime distribution of the emitters using the maximum entropy method. Based on the obtained lifetime distributions of the fluorophores, the ensemble-averaged fluorescence quantum yields have been estimated for IgG-FITC conjugates at various distances from Ag NP. And it was found that enhancement of FITC fluorescence near the colloidal particles was caused due to the change of the excitation efficiency rather than growth of the fluorescence quantum yield.

## Experimental methods

**Preparation of silver nanoparticles and films of polyelectrolytes.** The study has used phosphate buffered saline (PBS) with pH 7.4, silver nitrate, potassium citrate, polyelectrolytes (PE): polydiallyldimethylammonium chloride (PDADMAC) and polystyrene sulfonate, sodium salt (PSS), fluorescein isothiocyanate (FITC) and immunoglobulin G labelled by fluorescein isothiocyanate (the FITC:protein ratio=4), (IgG-FITC) (Aldrich, USA).

The films were applied using the glass substrates of the size of  $1 \times 2 \text{ cm}^2$ . The substrates were pre-washed in the  $\text{H}_2\text{O} + \text{H}_2\text{O}_2 + \text{NH}_3$  (1:1:1) mixture at  $70^\circ\text{C}$ , then the PDADMAC ( $M_w = 200000 \text{ g/mol}$ ) layer was deposited on them to impart a negative charge to the substrate surface. The silver nanoparticles were synthesized by citrate reduction of silver nitrate [32]. In accordance with the electron microscopy data, the average diameter of Ag NP in the sol was  $39 \pm 7 \text{ nm}$ . The negative charge of the silver particles caused by adsorption of the citrate ions makes it possible to electrostatically deposit them on the PDADMAC-modified substrates [33]. The alternating layers of PDADMAC and PSS in a number of 1 to 7 were formed on the surface of the produced silver films and the surface of the glass substrates [34]. Fig. 1 shows a scheme for preparing the samples of multi-layer films containing a labelled IgG-FITC protein and silver colloids. The film samples are designated under the following abbreviations: IgG-FITC/ $n$ PE/Ag (for the samples 1–4) and IgG-FITC/ $n$ PE (for the samples 5–8), where  $n$  — the number of the PDADMAC/PSS layers ( $n = 1–7$ ). The estimated thickness of the polyelectrolyte layer was 1.2–1.4 nm [34]. The top layer was always PDADMAC, the  $5 \mu\text{l}$  solution containing  $1 \mu\text{g}$  IgG-FITC, in the PBS buffer with pH 7.4 was applied thereon. The measurements were done in air in 30 min after the solution application.

The IgG-FITC from the solution was immobilized on the layer of the positively charged PDADMAC due to Coulomb

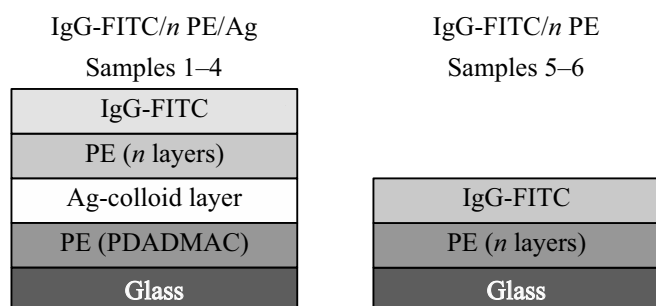


**Figure 1.** Scheme of preparing the multi-layer films containing the labelled IgG-FITC protein and silver nanoparticles. The number of the PDADMAC/PSS polyelectrolyte layers *n* is 1 (the samples 1, 5), 3 (the samples 2, 6), 5 (the samples 3, 7), 7 (the samples 4, 8).

**Table 1.** Distances between the layers of the Ag colloids and FITC in the samples of the metal-dielectric films

Sample	R(Ag–FITC), nm
IgG-FITC/ 1 PE/Ag	3.4 ± 2
IgG-FITC/ 3 PE/Ag	5.3 ± 2
IgG-FITC/ 5 PE/Ag	8.6 ± 2
IgG-FITC/ 7 PE/Ag	10.5 ± 2

interaction between the protein and the polyelectrolyte. The isoelectric point for the unmodified IgG is  $pI = 7 \pm 1$  and in the phosphate buffer with pH 7.4 used for solution preparation, the negative charge of the IgG-FITC protein molecule is determined by the presence of FITC dianion form available in its composition. The typical sizes of the IgG protein are  $14.5 \times 8.5 \times 4.0$  nm and it was assumed that after protein adsorption on the PDADMAC layer the protein molecules form a film of the thickness of  $\sim 4$  nm, i.e. uncertainty in localization of the FITC residues in the protein film is  $\pm 2$  nm. Based on the data about the thickness of the PDADMAC/PSS films [34] and the size of the IgG protein, the distances between the layers of colloidal Ag NPs and FITC in the film samples were evaluated (Table 1).

Fig. 2 shows the image of the IgG-FITC/1 PE film in a reflected light using the confocal microscope Nanofinder S (Solar, Belarus) and the fluorescence spectrum of IgG-FITC in the film.

**Measurements and analysis of the fluorescence kinetics data.** The fluorescence decay kinetics was measured by a pulsed fluorimeter using the time-correlated single photon counting (TCSPC) method. Fluorescence was excited using radiation of a pulsed laser diode with the wavelength of 467 nm, the duration of 70 ps and the pulse repetition rate of 20 MHz. The recording system included a PMA-182 photodetector unit, as well as TCSPC board TimeHarp 200 (PicoQuant, Germany). The scattered

exciting light was blocked using a Semrock long-pass edge filter designed to block radiation of  $\lambda < 500$  nm.

The fluorescence decay kinetics  $F(t)$  was determined in deconvolution of the experimental curves  $I(t)$ :

$$I(t) = \int_0^t IRF(t')F(t-t')dt', \quad (1)$$

where  $IRF(t)$  — an instrument response function of the spectrometer, using the software, described previously [35,36]. The duration of the instrument response function  $IRF(t)$  of the fluorimeter was  $\sim 300$  ps, but for the case of the monoexponential kinetics, the use of deconvolution makes it possible to achieve the time resolution of  $\sim 60$  ps [37]. The dependency of the function  $IRF$  on the wavelength (the PMT color effect) was taken into account by introducing a variable delay time  $\delta$  between  $IRF(t)$  and  $F(t)$ .

For analysis of the experimental data, the fluorescence decay function  $F(t)$  was represented as a sum of the exponents or a certain lifetime distribution of the emitting centers. In the case of the multiexponential model, the kinetics was described by a sum of the finite number of the exponential terms of the kind

$$F(t) = \sum_{i=1}^m \alpha_i \exp[-t/\tau_i], \quad (2)$$

where  $\alpha_i$ ,  $\tau_i$  — the pre-exponential factor (amplitude) and the lifetime of the *i*-th component of the fluorescence decay kinetics. The number of the exponents *m* was selected based on a condition of minimization of the reduced functional  $\chi_v^2$ :

$$\chi_v^2 = \frac{1}{\nu} \sum_{j=1}^N W_j [I(t_j) - I_{calc}(t_j)]^2, \quad (3)$$

where  $I(t_j)$  and  $I_{calc}(t_j)$  — the experimental and calculated values of the decay function for the time  $t_j$ ,  $W(t_j)$  — the corresponding statistical weight,  $\nu$  — the number of degrees of freedom, i.e. the difference of a number of the simulated data points *N* and a number of the varied parameters of the fitting function. In case of successful fitting using the multiexponential model, the value of the functional  $\chi_v^2$  should tend to 1, which was one of the goodness-of-fit criteria. The duration of the multiexponential kinetics was characterized by using the average values of the lifetimes  $\tau_\alpha$  and  $\langle \tau \rangle$ :

$$\tau_\alpha = \frac{\sum_{i=1}^m \alpha_i \tau_i}{\sum_{i=1}^m \alpha_i}, \quad (4)$$

$$\langle \tau \rangle = \frac{\sum_{i=1}^m \alpha_i \tau_i^2}{\sum_{i=1}^m \alpha_i \tau_i}, \quad (5)$$

where they are averaged, accordingly, by the amplitude and the weight of the exponential components  $S_i \sim \alpha_i \tau_i$  in emission.

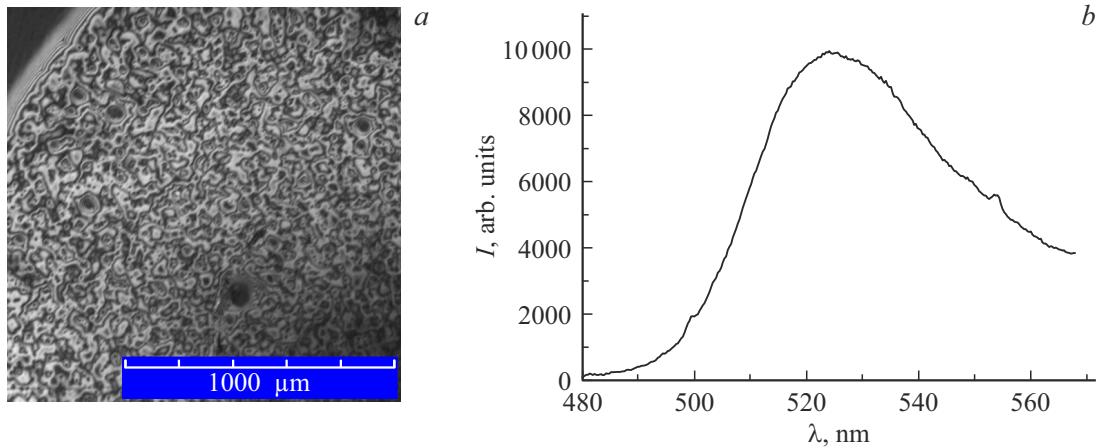


**Figure 2.** Image of the IgG-FITC/1 PE film in a reflected light as obtained using the confocal microscope Nanofinder S (Solar, Belarus) with the objective 10× (a) and the fluorescence spectrum of the labelled protein in the film composition (b).  $\lambda_{ex} = 473$  nm.

For the case of continuous lifetime distribution of the emitting centers, the fluorescence decay function  $F(t)$  was presented as

$$F(t) = \int_0^{\infty} \alpha(\tau) \exp[-t/\tau] d\tau, \quad (6)$$

where  $\alpha(\tau)$  — the unknown lifetime distribution of fluorophores. The distribution  $\alpha(\tau)$  was calculated using maximum entropy method (MEM) [38–43], which allows to reconstruct the most probable fluorophore distribution without a priori assumptions on a kind of the decay function. For this, searching  $\alpha(\tau)$ , besides minimization of the reduced functional  $\chi_v^2$ , includes maximization of the entropy function:

$$S = \int_0^{\infty} \left[ \alpha(\tau) - m(\tau) - \alpha(\tau) \log \frac{\alpha(\tau)}{m(\tau)} \right] d\tau, \quad (7)$$

where  $m(\tau)$  — the starting (prior) distribution characterizing the most probable a priori distribution of fluorophores. The optimal shape of the spectrum  $\alpha(\tau)$  under the condition  $\chi_v^2 \approx \chi_{v, \min}^2$  was determined by maximizing the magnitude  $\Psi$ :

$$\Psi = S - \mu(\chi_v^2 - \chi_{v, \min}^2), \quad (8)$$

where the regularization parameter  $\mu$  acts as a Lagrange multiplier, which modifies a contribution of the entropy-related summands  $S$  and  $\chi_v^2$  to the magnitude  $\Psi$ .

During kinetics analysis, the integral (6) has been replaced by the sum  $M$  of the exponential terms with the lifetimes which are logarithmically distributed with the step  $\Delta(\lg \tau)$  within the range  $[\tau_{\min}, \tau_{\max}]$ :

$$\lg \tau_i = \lg(\tau_{\min}) + (i - 1)\Delta(\lg \tau), \quad i = 1 \dots M. \quad (9)$$

For calculations it is convenient to convert to the logarithmic scale on lifetimes, since in this case the most probable

fluorophore distribution (without information about the decay kinetics) will be a uniform one [39]. In this case, with the replacement  $\alpha_i(\tau) = \alpha(\lg \tau_i)\Delta(\lg \tau)$ , the function  $F(t)$  is reduced to the expression (2), while the starting distribution model is determined as  $m(\lg \tau_i) = m_0$ , where  $m_0$  is the constant value.

Both the kind of the starting model and the value of  $m_0$  substantially affect reconstruction of the spectrum  $\alpha_i(\tau)$  [40,42,44,45]. First of all, the starting model was set by fitting the decay curve with the sum  $M$  of the exponentials with the lifetimes determined as per (9) and with common pre-exponential factors  $\alpha_0$ . Then the magnitude  $m_0$  was determined from the expression  $m_0 = \alpha_0/100$ .

The regularization parameter  $\mu$  was selected based on the dependency of the magnitude  $\chi_v^2$  on the value of  $\mu$  since for some experimental data the minimal value of  $\chi_{v, \min}^2$  (at  $\mu \gg 1$ ) substantially varied and did not approach 1. The first step included setting the value  $\mu = 100$  and searching for the distribution  $\alpha_i(\tau)$  and the delay time  $\delta$  that takes into account the dependency of the function  $IRF$  on the wavelength (the PMT color effect). Then, the found delay time  $\delta$  was fixed, and the kinetics was analyzed to calculate  $\chi_v^2$  value for the set of the values of  $\mu$  within the range from  $10^2$  to  $10^{-4}$ . The value  $\mu_c$ , which exhibited the change of a course of the dependency  $\chi_v^2(\mu)$ , was used for calculating the distribution  $\alpha(\lg \tau)$ . The software package for reconstruction of the lifetime distribution of fluorophores using maximum entropy method is described in more detail in the paper [36].

## Results and discussion

Fig. 3 shows fluorescence decay curves of IgG-FITC in the PBS solution and within multi-layer films containing the colloidal silver NPs. It can be seen that the immobilization of the labelled protein and its introduction into the composition of the multi-layer film results in substantial increase

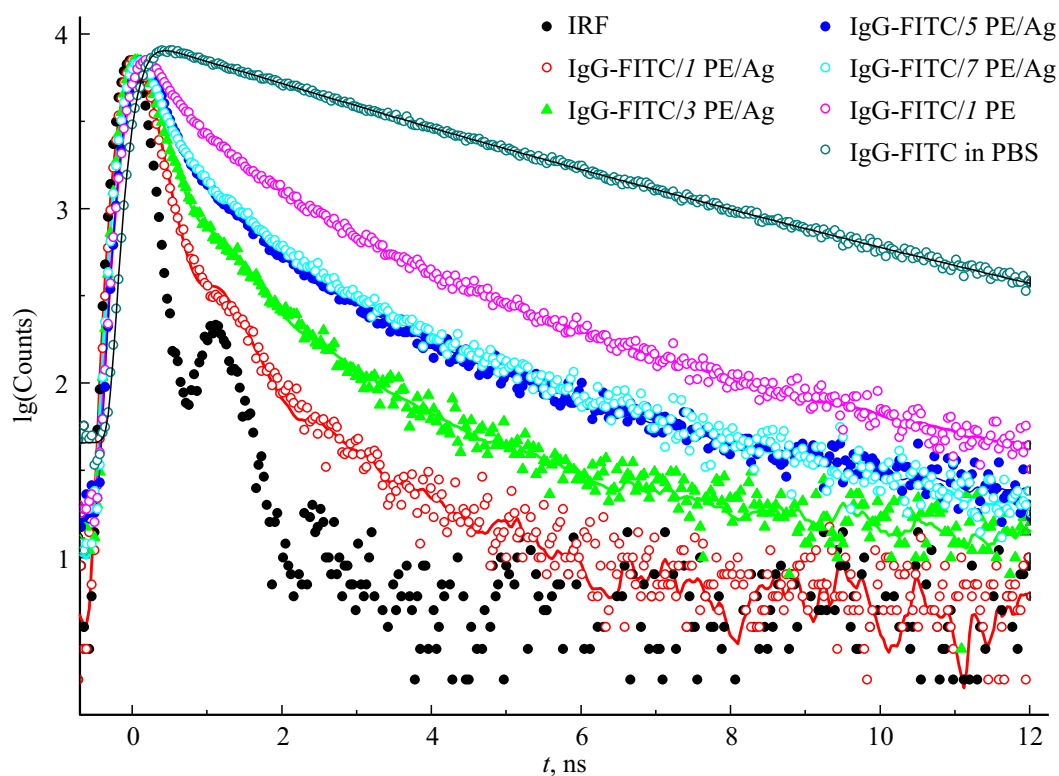


**Figure 3.** IgG-FITC fluorescence decay kinetics in the PBS solution and within the multi-layer films containing the colloidal Ag NPs.  $\lambda_{\text{ex}} = 467 \text{ nm}$ ,  $\lambda_{\text{fl}} = 520 \text{ nm}$ . The lines show the fitting of decay curves. IRF- instrument response function.

**Table 2.** Parameters of the fluorescence decay kinetics for free FITC and IgG-FITC in the PBS buffer with pH 7.4.  $\lambda_{\text{ex}} = 467 \text{ nm}$

Sample	$\lambda_{\text{fl}}$ , nm	$\alpha_1$	$\tau_1$ , ns	$S_1$ , %	$\alpha_2$	$\tau_2$ , ns	$S_2$ , %	$\langle \tau \rangle$ , ns	$\chi^2$
FITC	520	1	3.96	100				$3.96 \pm 0.08$	1.08
	550	1	3.94	100				$3.94 \pm 0.08$	1.12
	570	1	3.94	100				$3.94 \pm 0.08$	1.11
IgG-FITC	520	0.246	1.41	11.0	0.754	3.75	89.0	$3.50 \pm 0.07$	1.03
	540	0.241	1.36	10.3	0.759	3.77	89.7	$3.52 \pm 0.07$	1.12
	570	0.276	1.61	13.8	0.724	3.84	86.2	$3.53 \pm 0.07$	1.12

in a deactivation rate of the excited state of the fluorescent group.

The fluorescent properties of a fluorescein-based dyes substantially depend on pH [46], but in phosphate buffer at pH 7.4 the molecule of unbound FITC exists in the dianion form and its fluorescence decay kinetics is monoexponential with  $\tau \sim 3.9 \text{ ns}$  (Table 2). However, for IgG-FITC in the buffer, the fluorescence kinetics is biexponential with the lifetimes  $\sim 1.4$  and  $\sim 3.8 \text{ ns}$ , wherein the long-lived component has main contribution (89%) in emission (Table 2). The biexponential kinetics of fluorescence decay was observed for various proteins labelled by FITC [1,47–50], which was related to the presence of several binding centers of the label with different microenvironments [49]. With increase in the FITC:protein ratio, the decay kinetics nature becomes more complicated - triexponential [1,48] due to effects related to energy homotransfer and concentration

quenching of fluorescence. In our case, the number of the FITC groups per one protein molecule was  $n \sim 4$  for IgG-FITC, but the energy migration effects for the various FITC labels within the protein molecule are unimportant and the kinetic parameters almost do not depend on wavelength of the fluorescence (Table 2). Taking into account that the value of the Förster radius for energy migration (homotransfer) between fluorescein molecules is  $\sim 5 \text{ nm}$  [51], then it is probably related to significant size of the protein and the presence of more than 80 Lys residues, which can act as FITC binding centers [52].

Immobilization and introduction of IgG-FITC into the composition of the multi-layer film result in a reduced duration of emission decay and the kinetics can be satisfactorily described by means of at least three exponential components (Table 3). For the IgG-FITC/ $n$  PE films, lifetimes of the decay components take the values  $\tau_1 \sim 0.3\text{--}0.5 \text{ ns}$ ,

**Table 3.** Parameters of multiexponential fluorescence decay of IgG-FITC within the multi-layer films containing the silver colloids.  $\lambda_{\text{ex}} = 467 \text{ nm}$ ,  $\lambda_{\text{fl}} = 520 \text{ nm}$ 

Sample	$\alpha_1$	$\tau_1, \text{ ns}$	$S_1, \%$	$\alpha_2$	$\tau_2, \text{ ns}$	$S_2, \%$	$\alpha_3$	$\tau_3, \text{ ns}$	$S_3, \%$	$\tau_{\alpha}, \text{ ns}$	$\langle \tau \rangle, \text{ ns}$	$\chi^2$
IgG-FITC/1 PE/Ag	0.894	< 0.06	51.5	0.104	0.23	40.9	0.003	1.64	7.6	0.06	$0.24 \pm 0.12$	1.71
IgG-FITC/3 PE/Ag	0.906	< 0.06	35.2	0.087	0.30	44.0	0.008	1.63	20.9	0.06	$0.48 \pm 0.16$	1.27
IgG-FITC/5 PE/Ag	0.809	0.14	39.0	0.159	0.60	33.5	0.032	2.44	27.5	0.28	$0.93 \pm 0.10$	1.07
IgG-FITC/7 PE/Ag	0.791	0.14	35.0	0.173	0.63	35.5	0.036	2.53	29.5	0.31	$1.02 \pm 0.10$	1.34
IgG-FITC/1 PE	0.684	0.30	28.2	0.245	1.17	40.1	0.071	3.20	31.6	0.72	$1.56 \pm 0.10$	1.07
IgG-FITC/3 PE	0.625	0.34	21.9	0.261	1.36	36.8	0.115	3.48	41.3	0.96	$2.01 \pm 0.10$	1.02
IgG-FITC/5 PE	0.551	0.47	20.1	0.323	1.78	44.3	0.126	3.67	35.6	1.30	$2.19 \pm 0.10$	1.23
IgG-FITC/7 PE	0.644	0.41	28.1	0.243	1.36	35.0	0.113	3.08	36.9	0.94	$1.73 \pm 0.10$	1.06

$\tau_2 \sim 1.2\text{--}1.8 \text{ ns}$ ,  $\tau_3 \sim 3.1\text{--}3.7 \text{ ns}$ , while the amplitude-averaged  $\tau_{\alpha}$  and weight-averaged  $\langle \tau \rangle$  lifetimes vary within the ranges of 0.7–1.3 and 1.6–2.2 ns, respectively.

When silver colloids are present in the film composition, the average decay lifetime undergoes additional reduction, and one can see a significant correlation between the value of  $\langle \tau \rangle$  and the number  $n$  of the polyelectrolyte layers separating IgG-FITC from the silver colloids (Table 3). For example, for the IgG-FITC/7 PE/Ag sample, the average lifetime  $\langle \tau \rangle$  takes the value  $\sim 1 \text{ ns}$ , while for IgG-FITC/1 PE/Ag its value is reduced to  $\langle \tau \rangle \sim 0.2 \text{ ns}$ . The similar changes are also observed for the amplitude-averaged value of  $\tau_{\alpha}$ , which is proportional to the fluorescence quantum yield.

It is important to note that it is often difficult to ascribe a certain physical meaning to the parameters of the multiexponential kinetics, if the number of the kinetics components  $m \geq 3$ , and the studied fluorescent system has a high structural and dynamic heterogeneity. The similar situation is typical for the fluorescent labels or probes introduced in such macro- and supra-molecular systems as biopolymers, micelles, membranes, etc. These systems are characterized by high spatial heterogeneity and high conformation mobility. Fluorescence decay kinetics of fluorophores in such objects is substantially non-exponential, which is caused, on the one hand, by heterogeneity of the binding centers and their different microenvironment, and, on the other hand, by the influence of fluctuations of intermolecular interactions, nonstationary processes of relaxation, energy transfer, etc. In this case, more adequate approach to the studied system is description of the fluorescence decay using continuous lifetime distribution of the emitting centers [25,53].

The maximum entropy method was used for reconstruction of lifetime distributions of the emitting centers. The fluorophores distribution was represented as a set of 30 or 90 exponential components with the lifetimes values logarithmically distributed within the range of 0.04–10 ns, and the dependency  $\alpha(\lg \tau)$  was calculated. The regularization parameter  $\mu$  used in the calculation of the distribution shape was selected based on the dependency  $\chi_v^2$  on  $\mu$ .

The procedure for selecting the parameter  $\mu$  is exemplified as follows. Fig. 4, *a* shows a series of the distributions

$\alpha(\lg \tau)$  for the IgG-FITC solution in PBS buffer at various values of the regularization parameter  $\mu$ . Based on the change of the course of the dependency (Fig. 4, *b*), one has selected a value of the parameter  $\mu = \mu_c$ , starting from which the further growth of  $\mu$  did not result in substantial reduction of the value  $\chi_v^2$ . For the case of fluorescence kinetics for IgG-FITC in PBS, the regularization parameter was selected to be  $\mu_c = 0.03$ , while the distribution relevant thereto is shown on Fig. 4, *c*.

For the solution of FITC-labelled IgG protein in phosphate buffer at pH 7.4, MEM analysis can not resolve two exponential components in the kinetics with  $\tau_1 \sim 1.4 \text{ ns}$  and  $\tau_2 \sim 3.8 \text{ ns}$  (Table 2). And, since the long-lived component gives main contribution to the emission, the distributions  $\alpha(\lg \tau)$  are asymmetrically shaped with a peak at  $\tau \sim 3.8 \text{ ns}$  (Fig. 4, *c*). The second peak at  $\tau \sim 1.5 \text{ ns}$  in the distribution for IgG-FITC is revealed only when the regularization parameter is increased to the value  $\mu \geq 3$  (Fig. 4, *a*). Thus, level of accumulation of the kinetics data having Poissonian statistics and our approach used to determine the regularization parameter  $\mu_c$  could not allow to resolve the kinetics components with  $\tau_1 \sim 1.4 \text{ ns}$  and  $\tau_2 \sim 3.8 \text{ ns}$  as separate peaks. Nevertheless, the contribution of the short-lived component with  $\tau_1 \sim 1.4 \text{ ns}$  (Table 2) to fluorescence is taken into account in the analysis, thereby resulting in the asymmetry and broadening of the distribution. Specifically, the half-widths of the peaks of the distributions for IgG-FITC and free FITC in the solution are  $\Delta\tau \sim 2.1 \text{ ns}$  and  $\Delta\tau \sim 1.4 \text{ ns}$ , respectively, which are much higher than the duration of the instrument response function of the spectrometer ( $\sim 0.3 \text{ ns}$ ). Reconstruction of the distribution  $\alpha(\lg \tau)$  for the lifetimes range of 0.04–10 ns using 90 exponential components has negligible effect on the value of the peak half-width, so in the further calculations of the distributions we restricted ourselves in splitting of lifetime range into 30 components.

It is important to note that although the short- and long-lived components in the IgG-FITC kinetics with lifetimes  $\tau_1$  and  $\tau_2$  (Table 2) are not resolved as separate peaks, their contributions can be determined by decomposition of the

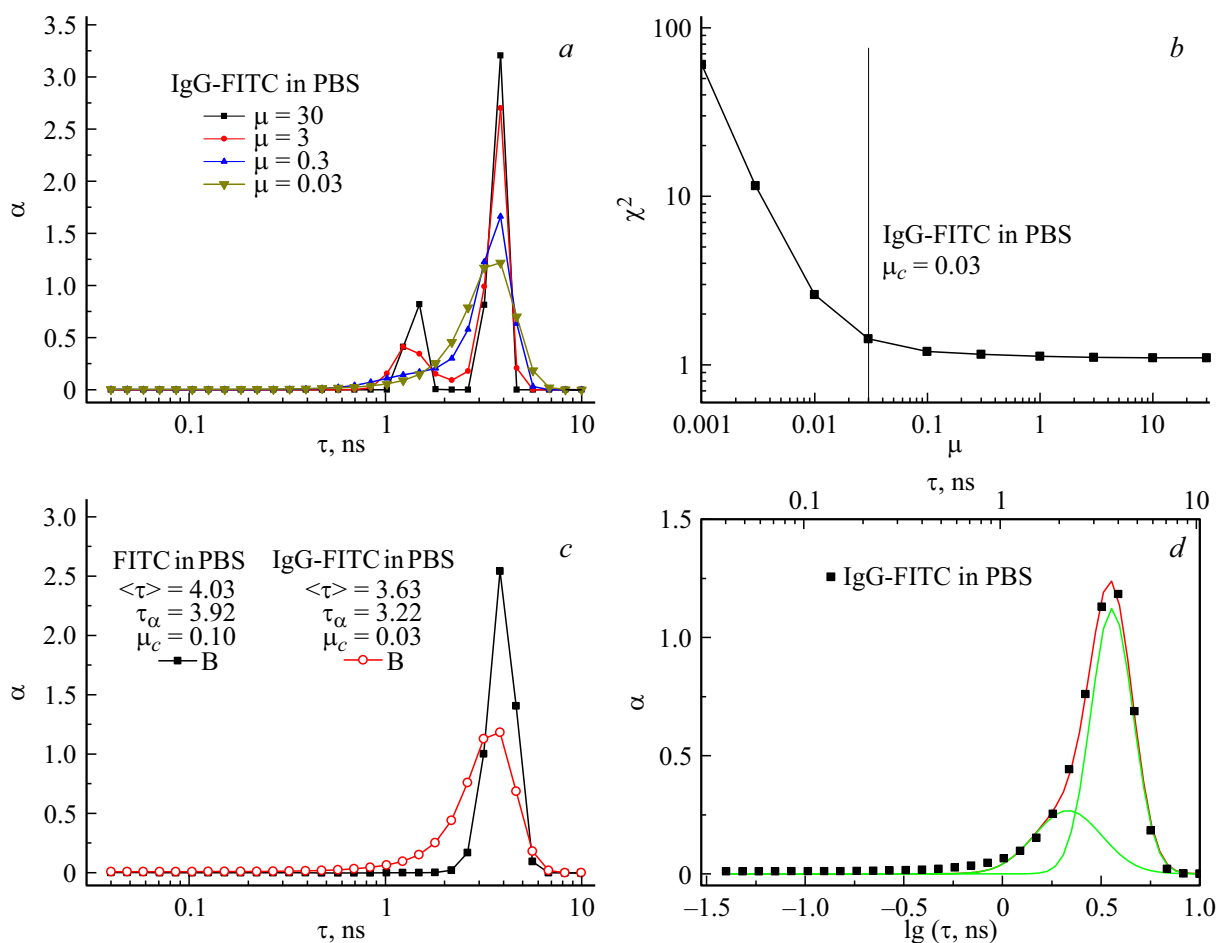


**Figure 4.** Lifetime distributions of the fluorophores for FITC and IgG-FITC in PBS solution.  $\lambda_{\text{ex}} = 473 \text{ nm}$ ,  $\lambda_{\text{fl}} = 520 \text{ nm}$ . *a* — the distributions  $\alpha(\lg \tau)$  for IgG-FITC at various values of the regularization parameter  $\mu$ ; *b* — the dependency  $\chi^2(\mu)$  for IgG-FITC indicating the critical value  $\mu_c = 0.03$ , *c* — lifetime distributions  $\alpha(\lg \tau)$  for FITC and IgG-FITC in PBS solution at  $\mu_c$ , equal to 0.1 and 0.03, respectively; *d* — the decomposition of the distribution  $\alpha(\lg \tau)$  for IgG-FITC in PBS solution into the Gaussians.

spectrum  $\alpha(\lg \tau)$  into Gaussians as follows

$$G(A_i, x_{0i}, \omega_i) = A_i / (w_i \sqrt{\pi/2}) \exp \left[ -2 \left( \frac{x - x_{0i}}{w_i} \right)^2 \right],$$

where  $A_i$ ,  $x_{0i}$ ,  $\omega_i$  — an area, a position and a parameter of the width for the  $i$ -th peak (Fig. 4, *d*, Table 4). When transitioning from the logarithmic scale  $\lg \tau$  to the linear one on  $\tau$ , it can be seen that the positions of the Gaussians  $\tau_{01} = 10^{x_{01}} = 2.1 \text{ ns}$  and  $\tau_{02} = 10^{x_{02}} = 3.6 \text{ ns}$ , as well as their areas ratio  $A_1/A_2 = 0.26/0.69$  well comply with the data of the biexponential decay kinetics for IgG-FITC (Table 2).

The shift and broadening of the lifetime distribution peak for the labelled IgG-FITC protein in comparison with the free FITC are mainly caused by the contribution of the short-lived component of the kinetics with  $\tau_1 \sim 1.4 \text{ ns}$  to fluorescence of the labelled protein (Table 2), as well as by heterogeneity of the FITC microenvironment within IgG, which affect the kinetic characteristics of the label fluorescence. However, there is neither spectral manifestation of the microenvironment heterogeneity for

different binding sites of the label in the protein, nor energy migration effects detected, and the lifetime distributions at various fluorescence wavelengths are almost the same, which complies with the data of Table 2.

Adsorption of IgG-FITC protein on surface of the multi-layer film results in changes of the fluorescence decay and shape of the lifetime distribution of the fluorophores (Fig. 5). Specifically, for the films without the silver colloids, the distribution exhibits an additional peak within the range of 0.3–0.5 ns (Fig. 5, *a*), in addition to the peak with the maximum at  $\tau \sim 3 \text{ ns}$ , which we relate to fluorescence of the FITC dianion form.

When considering the nature of the peak within the short lifetimes range in the lifetime distribution of fluorophores, it is necessary to take into account that the transition of the IgG-FITC protein from the solution into the solid-phase multi-layer film will result in a reduced distance between the FITC groups, belonging to the different protein molecules, due to a more compact packing of the protein in the film. It can result in fluorescence quenching due to aggregation of the chromophoric groups with formation

**Table 4.** Parameters of the Gaussians  $G(A, x_{0i}, w_i) = A_i/(w_i\sqrt{\pi/2}) \exp\left[-2\left(\frac{x-x_{0i}}{w_i}\right)^2\right]$  used for decomposition of the fluorophores distribution  $\alpha(\lg \tau)$  for IgG-FITC in the solution and within the multi-layer films. The brackets hold standard deviations.  $\lambda_{\text{ex}} = 467$  nm,  $\lambda_{\text{fl}} = 520$  nm

Sample	$A_1$	$x_{01}$	$w_1$	$A_2$	$x_{02}$	$w_2$
IgG-FITC in PBS	0.26 (0.16)	0.33(0.11)	0.34 (0.11)	0.69 (0.16)	0.56 (0.01)	0.21 (0.01)
IgG-FITC/ 1 PE	0.78 (0.01)	-0.503 (0.004)	0.49 (0.01)	0.21 (0.01)	0.24 (0.01)	0.45 (0.02)
IgG-FITC/ 3 PE	0.76(0.01)	-0.399 (0.006)	0.58 (0.01)	0.23 (0.01)	0.38 (0.01)	0.38 (0.02)
IgG-FITC/ 5 PE	0.73 (0.02)	-0.235 (0.008)	0.65 (0.02)	0.25 (0.02)	0.41 (0.01)	0.28 (0.01)
IgG-FITC/ 7 PE	0.78 (0.01)	-0.285 (0.004)	0.46 (0.01)	0.21 (0.01)	0.37 (0.01)	0.32 (0.02)
IgG-FITC/ 1 PE/Ag	0.92 (0.01)	-1.108 (0.002)	0.286 (0.003)	0.08 (0.01)	-0.57 (0.02)	0.32 (0.05)
IgG-FITC/ 3 PE/Ag	0.83 (0.02)	-1.089 (0.003)	0.317 (0.005)	0.16 (0.02)	-0.54 (0.03)	0.50 (0.06)
IgG-FITC/ 5 PE/Ag	0.72 (0.01)	-0.828 (0.001)	0.350 (0.004)	0.30 (0.02)	-0.49 (0.03)	1.09 (0.04)
IgG-FITC/ 7 PE/Ag	0.62 (0.02)	-0.904 (0.002)	0.348 (0.005)	0.40 (0.02)	-0.56 (0.03)	1.05 (0.03)

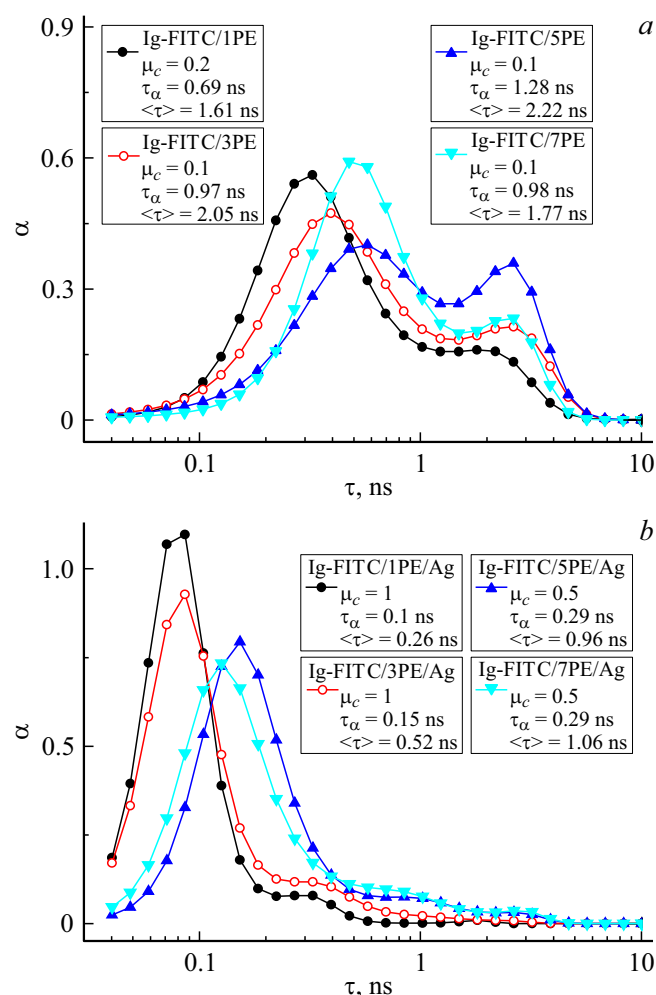


**Figure 5.** Lifetime distributions of fluorophores for IgG-FITC in the multi-layer film without the silver colloids (a) and at a different distance from the silver colloids (b).  $\lambda_{\text{ex}} = 467$  nm,  $\lambda_{\text{fl}} = 520$  nm.

of non-fluorescent dimers of FITC<sub>2</sub>, and due to increased efficiency of energy transfer processes among FITC residues in the protein film. It has been previously reported [47]

that decrease in the distance between separate FITC-labelled antibodies was accompanied by the reduction of fluorescence intensity and decay lifetime. For fluorescein-based dyes, the mechanism of concentration quenching of fluorescence is known [51], which consists in formation of the non-fluorescent fluorescein dimers upon increase of the dye concentration and the effective energy transfer from the monomers to the dimers. We suggest that appearance of the short-lifetime peak in the lifetime distribution  $\alpha(\lg \tau)$  is related to the processes of concentration quenching in the protein film. Besides, changes of the fluorophore microenvironment and interactions with the polar amino acids residues upon formation of the protein film will contribute to quenching of FITC fluorescence.

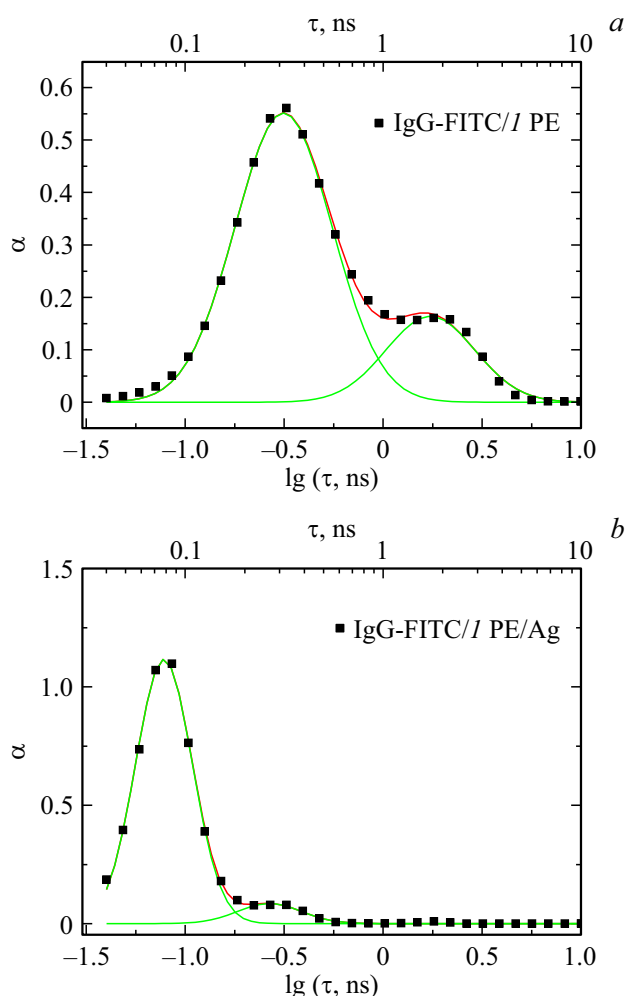
As the peaks in the bimodal distribution (Fig. 5, a) are partially overlapped, a portion of the fluorophores attributed to each peak was evaluated by decomposing the distribution into the Gaussians (Table 4). The decomposition into the Gaussians for the IgG-FITC/ 1 PE sample is shown on Fig. 6.

For the IgG-FITC samples in the films without silver colloids, the portion of the FITC fluorophores participating in energy transfer to the quencher (the non-fluorescent dimer FITC<sub>2</sub>) and attributed to the peak at  $\tau_{01} = 10^{x_{01}}$  within the region of the short lifetimes, was within the range from 0.73 to 0.78, thereby indicating high efficiency of energy transfer between the FITC residues in the multi-layer film (Table 5). However, the contribution to fluorescence  $S_i \sim \int \tau G_i(\lg \tau) d(\lg \tau)$  for the first group of the fluorophores was below 50%. For the second group of FITC residues, which are attributed to the peak at  $\tau_{02} = 10^{x_{02}}$ , we do not exclude occurrence of the energy migration processes, but the physical distance from the quenchers (the fluorescein dimers FITC<sub>2</sub>) results in the fact that they are deactivated predominantly by fluorescence emission.

The measured duration of fluorescence decay (decay lifetime of the excited state  $\tau$ ) is determined by the rate constant of the radiative transition  $k_r$  and the sum of the rate constants of all non-radiative transitions  $k_{nr}$  resulting in

**Table 5.** Parameters of lifetime distributions of fluorophores and the average values of the fluorescence quantum yields  $\langle\Phi\rangle$  for IgG-FITC in the multi-layer films without Ag NP.  $\lambda_{\text{ex}} = 467 \text{ nm}$ ,  $\lambda_{\text{fl}} = 520 \text{ nm}$ 

Samples	FITC residues, participating in energy transfer to FITC <sub>2</sub> quencher					FITC residues, that do not experience concentration quenching					Whole ensemble of FITC residues		
	$A_1$	$\tau_{01}$ , ns	$k_{nr01}$ , $10^9 \text{ s}^{-1}$	$\Delta k_{nr1}$ , $10^9 \text{ s}^{-1}$	$\langle\Phi\rangle_1$	$A_2$	$\tau_{02}$ , ns	$k_{nr02}$ , $10^9 \text{ s}^{-1}$	$\Delta k_{nr2}$ , $10^9 \text{ s}^{-1}$	$\langle\Phi\rangle_2$	$\langle\Phi\rangle$	$\langle\tau\rangle$ , ns	$\tau_\alpha$ , ns
IgG-FITC/1 PE	0.78	0.31	2.9	3.6	0.085	0.21	1.7	0.34	0.60	0.46	0.16	1.6	0.7
IgG-FITC/3 PE	0.76	0.40	2.3	3.3	0.11	0.23	2.4	0.19	0.36	0.61	0.22	2.0	1.0
IgG-FITC/5 PE	0.73	0.58	1.5	2.6	0.18	0.25	2.6	0.16	0.25	0.62	0.28	2.2	1.3
IgG-FITC/7 PE	0.78	0.52	1.7	2.0	0.14	0.21	2.3	0.20	0.31	0.58	0.22	1.8	1.0

**Figure 6.** Decomposition of the lifetime distribution  $\alpha(\lg \tau)$  into the Gaussian curves for IgG-FITC/1 PE (a) and IgG-FITC/1 PE/Ag (b).

deactivation of the excited state

$$\tau^{-1} = k_r + k_{nr}.$$

Taking into account value of the radiative transition rate constant for FITC dianion form  $k_r = 2.3 \cdot 10^8 \text{ s}^{-1}$  [46], one can obtain complete information about distribution of

fluorophores on non-radiative decay rate constant  $k_{nr}$  (i.e. information about the average value of  $k_{nr0}$  and its variation  $\Delta k_{nr}$ ) for the fluorophore groups IgG-FITC experiencing and not experiencing concentration quenching (Table 5), and about the average values of the fluorescence quantum yield. The values of the ensemble-averaged fluorescence quantum yield

$$\langle\Phi\rangle = \frac{k_r \int \tau_\alpha(\lg \tau) d(\lg \tau)}{\int \alpha(\lg \tau) d(\lg \tau)}, \quad (10)$$

and the similar values  $\langle\Phi\rangle_i$  for the  $i$ -th peak in the lifetime distribution of the fluorophores are shown in Table 5. The values  $\tau_\alpha$  and  $\langle\tau\rangle$  that characterize the average duration of the fluorescence kinetics and calculated based on the lifetime distribution of the fluorophores  $\alpha(\lg \tau)$  (Table 5) well comply with the results of the kinetics analysis using the multiexponential model (Table 3).

As can be seen, the average value of the fluorescence quantum yield  $\langle\Phi\rangle$  for IgG-FITC adsorbed onto the surface of the film without colloids is well correlated to the value  $\tau_\alpha$  and lies within the range of 0.2–0.3. It is significantly lower than the quantum yield for the free FITC in solution ( $\Phi = 0.93$ ) and is related to the effect of concentration quenching, which exhibits for 70–80% of the FITC residues. For the FITC residues experiencing concentration quenching, the average value of the quantum yield is reduced to  $\langle\Phi_1\rangle \sim 0.1$ –0.2. For the remaining FITC groups not experiencing concentration quenching, the value  $\langle\Phi_2\rangle$  is in  $\sim 3$ –5 times higher, but it does not reach 0.93, thereby possibly indicating change of the microenvironment and increase in interaction of the FITC residues with the protein side groups upon transition from the solution to the solid-phase film. The change in number of the polyelectrolyte layers in the films without the colloidal NPs results in a small variation of the kinetics parameters and the values  $\langle\Phi\rangle$ , but as there is no reason to expect a substantial change of the fluorescent properties for IgG-FITC in this case, this variation reflects, as we believe, the level of random error related to an unequal surface density of the protein in the films of different samples.

Presence of colloidal NPs in the film results in shifts of the peaks of the lifetime distribution of the emitting centers into the region of the smaller lifetimes (Fig. 5, b),

whereas the short-lifetime peak becomes dominant. The decomposition of the distribution  $\alpha(\lg \tau)$  into the Gaussians for the IgG-FITC/1 PE/Ag sample is shown on Fig. 6, while the parameters of the obtained Gaussians are given in Table 3.

For the IgG-FITC/1 PE/Ag film with minimal distance between the layers of Ag colloids and the labelled protein  $3.4 \pm 2$  nm, the portion of the fluorophores attributed to the first peak in the distribution at  $\tau_{m1} \sim 0.1$  ns (Fig. 5, 6, Table 6) is 0.92 and is gradually reduced to 0.62 with increasing the numbers of the polyelectrolyte layers which separate Ag NP and IgG-FITC. It indicates the substantial heterogeneity of the emitting centers and probably reflects the presence of a distance distribution between the colloidal NPs and FITC due to uncertainty in localization of the fluorescent group ( $\pm 2$  nm) within the protein molecule. It should be noted that  $\tau_{m1} \sim 0.1$  ns will be an upper estimate of the fluorescence decay lifetime for the fluorophores corresponding to the first peak in the distribution, as the time resolution of our spectrometer is also  $\sim 0.1$  ns, and in this case it is more correct to say that  $\tau_{m1} \leq 0.1$  ns.

If neglecting the possible change in the directional pattern of emission, then the fluorescence enhancement near the metal surfaces is related to the two factors [12,23,54]: 1) local electromagnetic field enhancement of the incident light wave near the metal nanostructures resulting in the growth of probability of fluorophore excitation, and 2) change of the quantum yield of the fluorescent object due to the change of probability of spontaneous optical transitions (the Purcell effect).

At the same time, the change of the quantum yield for fluorophore in the presence  $\Phi_M$  and in the absence  $\Phi_0$  of the metal nanostructures is determined from the expression [54]

$$\frac{\Phi_M}{\Phi_0} = \frac{\gamma_r}{(\gamma_r + k_{nr} + \gamma_{nr})} \frac{(k_r + k_{nr})}{k_r},$$

where  $\gamma_r$  — the radiative decay rate constant near the metal nanostructures,  $\gamma_{nr}$  — the radiative decay rate constant of energy transfer from the fluorophore to the metal colloids leading to fluorescence quenching. It is implicitly assumed that in the presence of the metal nanostructures the change of the magnitude  $k_{nr}$  of the fluorophore can be neglected. Within the framework of the mentioned model, the fluorescence decay kinetics near the metal nanostructures is characterized by the lifetime  $\tau = (\gamma_r + \gamma_{nr} + k_{nr})^{-1}$ .

The determination of  $\gamma_r$  or  $\gamma_{nr}$  requires independent experimental data on the value of the fluorescence quantum yield, whose measurement is technically challenged for the studied systems in the films. For this reason we have evaluated the value of the rate constant of the radiative transition  $\gamma_r$  in the presence of the colloids based on the calculations with the framework of the previously described theoretical model [12].

Fig. 7 shows the relative value of the change of the orientation-averaged rate constant of the radiative transition  $\langle \gamma_r/k_r \rangle$  for the fluorescent molecule at the distance  $\Delta r$  to

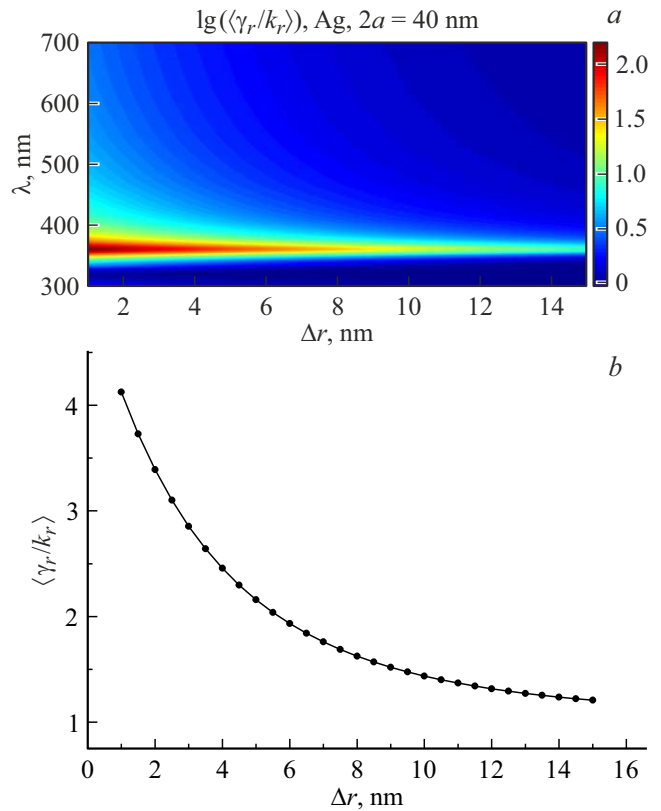


**Figure 7.** *a* — the change of decadic logarithm of the ratio of the orientation-averaged radiative transition rate constants  $\gamma_r/k_r$ , depending on fluorescence wavelength and distance to a silver spherical particle with size of 40 nm. *b* — the dependency of the ratio of the orientation-averaged rate constants of the radiative transition  $\gamma_r/k_r$  on the distance between a fluorophore and Ag nanoparticle with size of 40 nm.

the spherical Ag nanoparticle of the size of 40 nm in air for different wavelengths. Based on the dependency of the value  $\langle \gamma_r/k_r \rangle$  at 520 nm, where maximum of FITC fluorescence is located (Fig. 7, *b*) and on the distance between the layers of Ag NP and FITC (Table 1), one can evaluate the value of the rate constant of the radiative transition  $\gamma_r$  for IgG-FITC within the metal-dielectric film (Table 6) and the average values of the fluorescence quantum yield using the expression (10).

As can be seen from Table 6, the average value of the fluorescence quantum yield  $\langle \Phi \rangle$  for the whole ensemble of the FITC fluorophores in the film with colloids does not exceed the value  $\langle \Phi \rangle = 0.11$ , i.e. the effect of Ag NP ( $d = 40$  nm) does not result in increase of the quantum yield and it is in  $\sim 2$  times lower than the similar value  $\langle \Phi \rangle$  for the films without colloids (Table 5). Thus, the peak in the lifetime distribution  $\alpha(\lg \tau)$  at  $\tau_{m1} \sim 0.1$  ns corresponds to the group of FITC molecules experiencing fluorescence quenching  $\langle \Phi_1 \rangle \leq 0.06$  due to effective energy transfer to Ag NPs with subsequent dissipation into heat. For the second group of fluorophores, in the lifetime distribution with the peak at  $\tau_{m2} \sim 0.3$  ns, the value of  $\langle \Phi_2 \rangle$

**Table 6.** Parameters of the fluorescence kinetics for the IgG-FITC in the multi-layer films with colloids.  $\lambda_{\text{ex}} = 467 \text{ nm}$ ,  $\lambda_{\text{fl}} = 520 \text{ nm}$ 

Samples	$\gamma_r, 10^9$ $\text{s}^{-1}$	1 <sup>st</sup> peak			2 <sup>nd</sup> peak			All FITC residues		
		$A_1$	$\tau_{m1}, \text{ns}$	$\langle \Phi_1 \rangle$	$A_2$	$\tau_{m2}, \text{ns}$	$\langle \Phi_2 \rangle$	$\tau_\alpha, \text{ns}$	$\langle \tau \rangle, \text{ns}$	$\langle \Phi \rangle$
IgG-FITC/ 1 PE/Ag	0.60	0.92	0.08	0.05	0.08	0.27	0.17	0.1	0.26	0.06
IgG-FITC/ 3 PE/Ag	0.46	0.83	0.08	0.04	0.16	0.29	0.16	0.15	0.52	0.07
IgG-FITC/ 5 PE/Ag	0.37	0.72	0.15	0.06	0.30	0.32	0.26	0.29	0.96	0.11
IgG-FITC/ 7 PE/Ag	0.32	0.62	0.12	0.04	0.40	0.28	0.18	0.29	1.06	0.09

is in  $\sim 4$  times higher and the maximum of quantum yield is observed at the average distance  $8.6 \pm 2 \text{ nm}$  between the FITC layers and the colloidal Ag NPs.

Thus, the obtained results indicate that the enhancement of FITC fluorescence in the presence of Ag NPs with  $d = 40 \text{ nm}$ , as previously reported [17], is caused not by increase in the fluorescence quantum yield of FITC, but it is mainly related to increase in probability of the fluorophores excitation in the presence of the colloidal Ag NPs.

## Conclusions

We have experimentally investigated fluorescence decay kinetics of IgG-FITC conjugates immobilized on the surface of metal-dielectric films, wherein the protein layer and the layer of colloidal Ag NPs with size of  $40 \text{ nm}$  were spaced apart by the alternating PDADMAC/PSS polyelectrolyte layers with a number of the layers from 1 to 7. Transition of IgG-FITC from buffer solution into the solid-phase dielectric film formed by PDADMAC/PSS polyelectrolytes results in the change of fluorescence decay kinetics due to manifestation of the effects of concentration quenching. It was found that duration of fluorescence decay kinetics of IgG-FITC in metal-dielectric films depended on the distance between the layers of the colloidal Ag NPs and the labelled protein.

In order to interpret the obtained results, fluorescence decay curves of FITC were analyzed using continuous lifetime distribution of the emitters using the maximum entropy method. Dependence of the radiative transition rate constant for FITC on the distance from FITC to metal NP has been evaluated using the previously published theoretical model [12]. Based on the obtained lifetime distributions of the fluorophores  $\alpha(\lg \tau)$ , ensemble-averaged fluorescence quantum yields for IgG-FITC conjugates in films at various distances to the plasmonic silver layer have been evaluated. And it has been found that the enhancement of FITC fluorescence near colloidal NPs is not related to growth of the fluorescence quantum yield (as increase in  $\gamma_r$  is compensated by a stronger increase in rate constant of non-radiative transition  $\gamma_{nr}$ ), but it is caused by the excitation efficiency change due to the local enhancement of the light wave field. The maximum of IgG-FITC quantum yield was observed at the average distance of  $8.6 \pm 2 \text{ nm}$  between FITC and the silver plasmonic film.

## Acknowledgments

The authors would like to thank I.V. Koktysh and Ya.I. Melnikova for discussion of the work results and their help in preparation of the samples for study, I.G. Motevich for performing some spectral measurements, and A.A. Romanenko for valuable discussion of the study results.

## Funding

The International Sakharov Environmental Institute of Belarusian State University would like to thank the Belarusian Republican Foundation for Fundamental Research (the project № F22TURT-007) and Ministry of Education of the Republic of Belarus (the State Research Programs of the Republic of Belarus „Photonics and Electronics for Innovation“, Assignment 1.5).

## Conflict of interest

The authors declare that they have no conflict of interest.

## References

- [1] J.R. Lakowicz, J. Malicka, S. D'Auria, I. Gryczynski. *Anal Biochem.*, **320** (1), 13 (2003). DOI: 10.1016/S0003-2697(03)00351-8
- [2] O. Kulakovich, N. Strekal', M. Artem'ev, A. Stupak, S. Maskevich, S. Gaponenko. *J. Appl. Spectrosc.*, **73** (6), 892 (2006). DOI: 10.1007/s10812-006-0172-3.
- [3] K. Kneipp. *Physics Today*, **60** (11), 40 (2007). DOI: 10.1063/1.2812122
- [4] M.I. Stockman. *Physics Today*, **64** (2), 39 (2011). DOI: 10.1063/1.3554315
- [5] A. Steinbrück, A. Csaki, W. Fritzsche. *Reviews in Plasmonics 2010* (NY: Springer New York, 2012), p. 1. DOI: 10.1007/978-1-4614-0884-0\_1
- [6] N. Strekal, S. Maskevich. *Reviews in Plasmonics 2010* (NY: Springer New York, 2012), p. 283. DOI: 10.1007/978-1-4614-0884-0\_11
- [7] A. Ramanenka, S. Vaschenko, V. Stankevich, A.Y. Lunevich, Y.F. Glukhov, S. Gaponenko. *J. Appl. Spectrosc.*, **81** (2), 222 (2014). DOI: 10.1007/s10812-014-9913-x.
- [8] J. Luan, A. Seth, R. Gupta, Z. Wang, P. Rathi, S. Cao, H. Gholami Derami, R. Tang, B. Xu, S. Achilefu, J.J. Morrissey, S. Singamaneni. *Nature Biomedical Engineering*, **4** (5), 518 (2020). DOI: 10.1038/s41551-020-0547-4

- [9] V. Askirka, D. Guzatov, S. Maskevich. *Opt. Spectrosc.*, **129**, 261 (2021). DOI: 10.1134/S0030400X21020028.
- [10] M. Wang, M. Wang, G. Zheng, Z. Dai, Y. Ma. *Nanoscale Advances*, **3** (9), 2448 (2021). DOI: 10.1039/D0NA01050B
- [11] N. Strekal, O. Kulakovich, V. Askirka, I. Sveklo, S. Maskevich. *Plasmonics*, **4** (1), 1 (2009). DOI: 10.1007/s11468-008-9063-1
- [12] D.V. Guzatov, S.V. Vaschenko, V.V. Stankevich, A.Y. Lunevich, Y.F. Glukhov, S.V. Gaponenko. *J. Phys. Chem. C*, **116** (19), 10723 (2012). DOI: 10.1021/jp301598w
- [13] A. Muravitskaya, O. Kulakovich, P.M. Adam, S. Gaponenko. *Phys. Stat. Sol. B*, **255** (4), 1700491 (2018). DOI: 10.1002/pssb.201700491
- [14] S. Vaschenko, A. Ramanenka, O. Kulakovich, A. Muravitskaya, D. Guzatov, A. Lunevich, Y. Glukhov, S. Gaponenko. *Proc. Engin.*, **140**, 57 (2016). DOI: 10.1016/j.proeng.2015.08.1111
- [15] I. Koktysh, Y.I. Melnikova, O. Kulakovich, A. Ramanenka, S. Vaschenko, A. Muravitskaya, S. Gaponenko, S. Maskevich. *J. Appl. Spectrosc.*, **87**, 870 (2020). DOI: 10.1007/s10812-020-01083-2.
- [16] O. Kulakovich, A. Scherbovich, I. Koktysh, Y. Melnikova, A. Ramanenka, S. Gaponenko, S. Maskevich. *Z. Phys. Chem.*, **236** (11–12), 1603 (2022). DOI: 10.1515/zpch-2021-3110
- [17] O. Kulakovich, A. Shcherbovich, A. Ramanenka, I. Koktysh, Y.I. Melnikova, S. Gaponenko, S. Maskevich. *J. Appl. Spectrosc.*, **90** (1), 42 (2023). DOI: 10.1007/s10812-023-01500-2.
- [18] S.V. Gaponenko, D.V. Guzatov. *Proc. IEEE*, **108** (5), 704 (2020). DOI: 10.1109/jproc.2019.2958875
- [19] D.V. Guzatov, S.V. Gaponenko, H.V. Demir. *AIP Advances*, **8** (1), 015324 (2018). DOI: 10.1063/1.5019778
- [20] X. Yang, P.L. Hernandez-Martinez, C. Dang, E. Mutlugun, K. Zhang, H.V. Demir, X.W. Sun. *Advanced Opt. Mater.*, **3** (10), 1439 (2015). DOI: 10.1002/adom.201500172
- [21] Z. Lei, M. Liu, W. Ge, X. Yang, J. Chen, Y. Lu. *J. Lumin.*, **206**, 359 (2019). DOI: 10.1016/j.jlumin.2018.10.052
- [22] A.P. Demchenko. *Introduction to fluorescence sensing* (Cham: Springer, 2015). DOI: 10.1007/978-3-319-20780-3
- [23] M. Bauch, K. Toma, M. Toma, Q. Zhang, J. Dostalek. *Plasmonics*, **9**, 781 (2014). DOI: 10.1007/s11468-013-9660-5
- [24] A.B.T. Ghisaidoobe, S.J. Chung. *International J. Mol. Sci.*, **15** (12), 22518 (2014). DOI: 10.3390/ijms151222518
- [25] J.R. Alcala, E. Gratton, F. Prendergast. *Biophys. J.*, **51** (4), 597 (1987). DOI: 10.1016/S0006-3495(87)83384-2
- [26] E.P. Diamandis. *Clin. Biochem.*, **21** (2), 139 (1988). DOI: 10.1016/0009-9120(88)90001-x
- [27] A.K. Hagan, T. Zuchner. *Anal. Bioanal. Chem.*, **400** (9), 2847 (2011). DOI: 10.1007/s00216-011-5047-7
- [28] H. Mishra, B.L. Mali, J. Karolin, A.I. Dragan, C.D. Geddes. *PCCP*, **15** (45), 19538 (2013). DOI: 10.1039/C3CP50633A
- [29] Y.-T. Liu, X.-F. Luo, Y.-Y. Lee, I.-C. Chen. *Dyes and Pigments*, **190**, 109263 (2021). DOI: 10.1016/j.dyepig.2021.109263
- [30] J.S. Beckwith, C.A. Rumble, E. Vauthey. *Int. Rev. Phys. Chem.*, **39** (2), 135 (2020). DOI: 10.1080/0144235X.2020.1757942
- [31] N. Dordević, J.S. Beckwith, M. Yarema, O. Yarema, A. Rosspeintner, N. Yazdani, J. Leuthold, E. Vauthey, V. Wood. *ACS Photonics*, **5** (12), 4888 (2018). DOI: 10.1021/acsp Photonics.8b01047
- [32] P.C. Lee, D. Meisel. *J. Phys. Chem.*, **86** (17), 3391 (1982). DOI: 10.1021/j100214a025
- [33] O. Kulakovich, L. Gurinovich, H. Li, A. Ramanenka, L. Trotsiuk, A. Muravitskaya, J. Wei, H. Li, N. Matveevskaya, D.V. Guzatov, S. Gaponenko. *Nanotechnology*, **32** (3), 035204 (2021). DOI: 10.1088/1361-6528/abbdde
- [34] F. Caruso. *Adv. Mater.*, **13** (1), 11 (2001). DOI: 10.1002/1521-4095(200101)13:1;1-11::AID-ADMA11;3.0.CO;2-N
- [35] V. Stepuro. *Vesnik Grodzenskaga dzyarzhauaga universiteta imya Yanki Kupaly. Seryya 2*, **5** (1), 52 (2001) (in russian).
- [36] A. Maskevich, V. Stsiapura, P. Balinski. *J. Appl. Spectrosc.*, **77** (2), 194 (2010). DOI: 10.1007/s10812-010-9314-8.
- [37] A. Maskevich, V. Stepuro, S. Kurguzenkov, A. Lavysh. *Vesnik Grodzenskaga dzyarzhauaga universiteta imya Yanki Kupaly. Seryya 2*, **3** (159), 107 (2013) (in russian).
- [38] M. Vincent, J. Gallay, A.P. Demchenko. *J. Phys. Chem.*, **99** (41), 14931 (1995). DOI: 10.1021/j100041a006
- [39] A. Livesey, J. Brochon. *Biophys. J.*, **52** (5), 693 (1987). DOI: 10.1016/S0006-3495(87)83264-2
- [40] J.-C. Brochon. *Methods Enzymol.*, **240**, 262 (1994). DOI: 10.1016/s0076-6879(94)40052-0
- [41] A. Siemiarz, B.D. Wagner, W.R. Ware. *J. Phys. Chem.*, **94** (4), 1661 (1990). DOI: 10.1021/j100367a080
- [42] P.J. Steinbach, R. Ionescu, C.R. Matthews. *Biophys. J.*, **82** (4), 2244 (2002). DOI: 10.1016/S0006-3495(02)75570-7
- [43] R. Esposito, C. Altucci, R. Velotta. *J. Fluoresc.*, **23** (1), 203 (2013). DOI: 10.1007/s10895-012-1135-0
- [44] A.T. Kumar, L. Zhu, J. Christian, A.A. Demidov, P.M. Champion. *J. Phys. Chem. B*, **105** (32), 7847 (2001). DOI: 10.1021/jp0101209
- [45] E. Henry, E. Deprez, J.-C. Brochon. *J. Mol. Struct.*, **1077**, 77 (2014). DOI: 10.1016/j.molstruc.2013.12.079
- [46] R. Sjöback, J. Nygren, M. Kubista. *Spectrochim. Acta Part A: Molecular and Biomolecular Spectrosc.*, **51** (6), L7 (1995). DOI: 10.1016/0584-8539(95)01421-P
- [47] C. Deka, B.E. Lehnert, N.M. Lehnert, G.M. Jones, L.A. Sklar, J.A. Steinkamp. *Cytometry*, **25** (3), 271 (1996). DOI: 10.1002/(SICI)1097-0320(19961101)25:3;271::AID-CYTO8;3.0.CO;2-I
- [48] G. Hungerford, J. Benesch, J.F. Mano, R.L. Reis. *Photochem. & Photobiolog. Sci.*, **6** (2), 152 (2007). DOI: 10.1039/b612870j
- [49] E. Grell, E. Lewitzki, H. Ruf, K. Brand, F.W. Schneider, T. von der Haar, K.A. Zachariasse. *J. Fluoresc.*, **4** (3), 251 (1994). DOI: 10.1007/bf01878459
- [50] E. Lewitzki, E. Schick, R. Hutterer, F.W. Schneider, E. Grell. *J. Fluoresc.*, **8** (2), 115 (1998). DOI: 10.1023/a:1022542208027
- [51] R.F. Chen, J.R. Knutson. *Anal. Biochem.*, **172** (1), 61 (1988). DOI: 10.1016/0003-2697(88)90412-5
- [52] P. Denner, E. Fischer, R. Schibli. *Antibodies*, **4** (3), 197 (2015). DOI: 10.3390/antib4030197
- [53] K. Palo, L. Brand, C. Eggeling, S. Jäger, P. Kask, K. Gall. *Biophys. J.*, **83** (2), 605 (2002). DOI: 10.1016/s0006-3495(02)75195-3
- [54] O. Kulakovich, S. Gaponenko, D. Guzatov. *J. Appl. Spectrosc.*, **90** (3), 567 (2023). DOI: 10.1007/s10812-023-01567-x.

Translated by M.Shevelev